Structure
Article

Open-State Conformation of the KcsA K^+ Channel: Monte Carlo Normal Mode Following Simulations

Gennady V. Miloshevsky[1] and Peter C. Jordan[1,*]
[1]Department of Chemistry, MS-015, Brandeis University, P.O. Box 549110, Waltham, MA 02454-9110, USA
*Correspondence: jordan@brandeis.edu
DOI 10.1016/j.str.2007.09.022

SUMMARY

Potassium channels fluctuate between closed and open states. The detailed mechanism of the conformational changes opening the intracellular pore in the K^+ channel from *Streptomyces lividans* (KcsA) is unknown. Applying Monte Carlo normal mode following, we find that gating involves rotation and unwinding of the TM2 bundle, lateral movement of the TM2 helices away from the channel axis, and disappearance of the TM2 bundle. The open-state conformation of KcsA exhibits a very wide inner vestibule, with a radius ~5–7 Å and inner helices bent at the A98–G99 hinge. Computed conformational changes demonstrate that spin labeling and X-ray experiments illuminate different stages in gating: transition begins with clockwise rotation of the TM2 helices ending at a final state with the TM2 bend hinged near residues A98–G99. The concordance between the computational and experimental results provides atomic-level insights into the structural rearrangements of the channel's inner pore.

INTRODUCTION

During a process called gating, the K^+ channel from *Streptomyces lividans* (KcsA) (Doyle et al., 1998) undergoes a conformational change that opens the intracellular (IC) pore. This process, a transition between a closed and open state, is not fully understood atomistically. The essential movement of the transmembrane TM1 and TM2 helices found in spin labeling and electron paramagnetic resonance (EPR) experiments (Perozo et al., 1999; Liu et al., 2001) was clockwise rotation relative to the channel axis (Perozo et al., 1999) when viewed from the IC side, twisting TM2 (~30°) about the helical axis (Liu et al., 2001). In this rotation-and-tilt mechanism, the pore diameter at the IC end of KcsA was as large as 10 Å, while the diameter of the inner hydrophobic vestibule around residues T107 and A108 only increased by ~2 Å. Structural comparison of the IC halves of the TM2 helices in a closed channel, KcsA, and an open channel, MthK, suggested a hinge-bending mechanism (Jiang et al., 2002), where the main conformational change during gating was a substantial outward-directed bend (~30°) of the TM2 helices at a hinge point corresponding to G99 in KcsA and G83 in MthK. The TM2 helices splayed open and the bundle crossing disappeared. The IC pore was ~12 Å wide at its narrowest point (A88-MthK), with the central cavity becoming an integral part of the IC solution (Jiang et al., 2002).

Because the conformation of the TM2 bundle is very different in the rotation-and-tilt and hinge-bending models, they were viewed as effectively incompatible proposals (Kelly and Gross, 2003). The key differences in analysis of these models (Perozo, 2002) are the presence of a gating hinge in MthK at the conserved glycine and an increase of ~12 Å in the inner vestibule of the pore. While there is considerable controversy regarding the nature, location, and magnitude of molecular movements, both proposals agree that channel opening requires clockwise (viewed from the IC side) rotation of the TM2 helices. It is important to stress the following two points: (1) as the open-state probability of KcsA channel remains very low, even at acidic pH (Cuello et al., 1998; Heginbotham et al., 1999), spin labeling and EPR spectroscopy (Perozo et al., 1999; Liu et al., 2001) might describe structural dynamics in the early stages of opening the TM2 bundle (Perozo, 2002); and (2) comparing the two channels—closed, pH-dependent KcsA (Doyle et al., 1998) and opened, ligand-gated MthK (Jiang et al., 2002)—the hinge-bending model identifies distinct end-point conformers, but provides no way to determine mechanistic details of the structural change. Is it possible that the rotation-and-tilt model describes the dynamics initiating gating (Perozo, 2002) and the hinge-bending model provides an end-state picture of the open channel?

It is now accepted, both experimentally and theoretically, that low-frequency normal modes (NMs) govern the large-scale conformational transitions that are vital for protein functioning. Phonon-assisted Mössbauer measurements on myoglobin (Achterhold et al., 2002) demonstrate that: (1) harmonic low-temperature dynamics remain manifest at physiological temperatures; and (2) room-temperature quasidiffusive transitions follow pathways determined by the harmonic motions. In standard NM analysis (NMA) (Levitt et al., 1985), the direction prescribed by the lowest-frequency NM is associated with the gating pathway. NMA has successfully been used to identify large-scale motions in protein channels, such as KcsA (Shen et al., 2002; Shrivastava and Bahar, 2006), MscL (Valadie et al., 2003), and nAChR (Taly et al.,

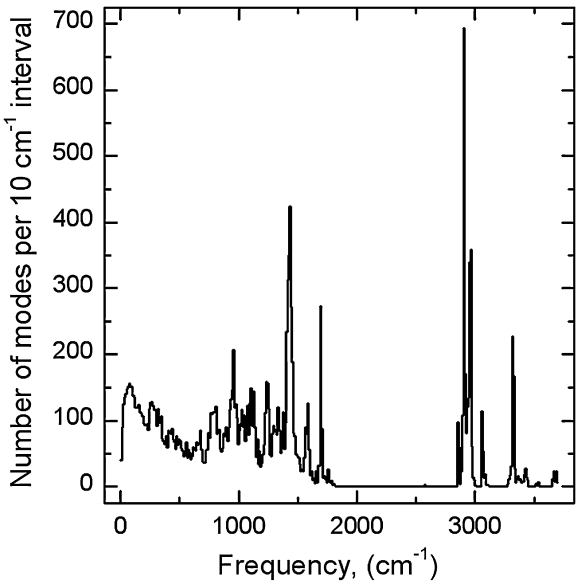

Figure 1. The Frequency Spectrum of the WT KcsA System
The lowest-frequency eigenvalue is 2.64 cm^{-1}. The region <500 cm^{-1} describes concerted motions of secondary structure elements (α helices and large groups of amino acids). The region from 500 to 1830 cm^{-1} corresponds to internal vibrations of single amino acids (torsional motions, with valence angle and bond vibrations near the high-frequency end of this region). The well-separated block >2840 cm^{-1} corresponds to hydrogen-heavy atom vibrations.

2005; Cheng et al., 2006). In these NMA studies, a target structure is generated from an initial structure via a single-step atomic displacement along the lowest-frequency NM eigenvector until a preset rmsd, typically 2.0–3.5 Å, between the two structures is attained. Recently, we developed a Monte Carlo NM following (MC-NMF) method (Miloshevsky and Jordan, 2006), combining NMA (Levitt et al., 1985) and the eigenvector following approach (Nichols et al., 1990) with the Metropolis Monte Carlo (MC) method (Metropolis et al., 1953). It differs crucially from standard NMA in that the intermediate structures on the gating pathway are generated by constructing a properly ordered sequence of small steps moving energetically uphill along the lowest-frequency NM, simultaneously minimizing the energy along all other orthogonal modes (Nichols et al., 1990). We have simulated opening the IC pore in KcsA by means of an MC-NMF technique developed earlier to reveal the gating mechanism of the gramicidin A (gA) open state (Miloshevsky and Jordan, 2006). The MC-NMF method has been previously described in detail (Miloshevsky and Jordan, 2006). The modifications needed in application to KcsA, using a rotation-translation of blocks (RTB) approximation (Tama et al., 2000), are presented in Experimental Procedures.

RESULTS

Lowest-Frequency NM of KcsA from All-Mode NMA

All-atom NMA calculations were performed for wild-type (WT) KcsA and three variants protonating either or both sets of residues, E118 and E120 (termed E118p KcsA, E120p KcsA, and E118p/E120p KcsA, respectively). The calculated NM frequency spectrum is shown in Figure 1 for the WT KcsA system. In all four KcsA systems, the NM frequency spectrum and the lowest-frequency eigendirection were nearly the same. Which KcsA domains move along the lowest-frequency NM vector and what are the associated conformational changes? Figure 2 illustrates perturbation of the minimized WT KcsA structure along the lowest-frequency eigenvector. This NM reveals

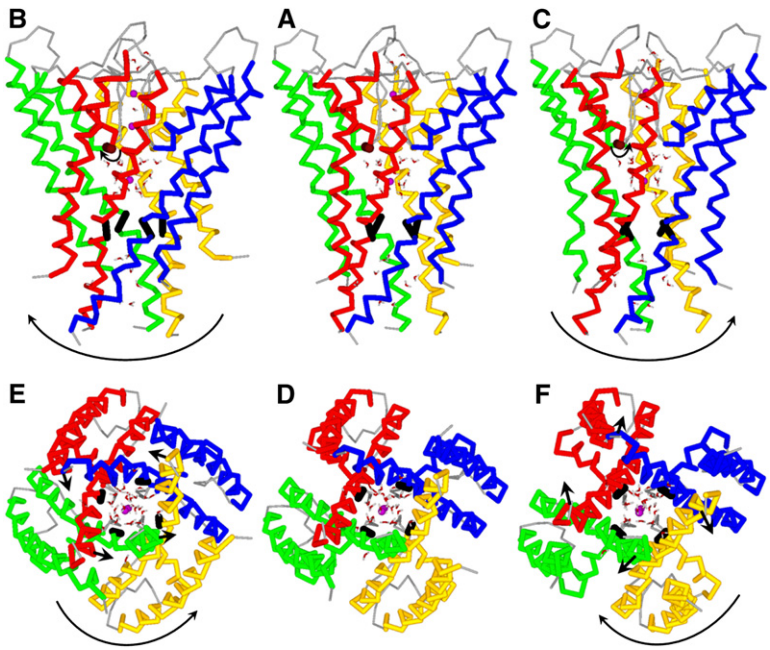

Figure 2. Perturbation of the WT KcsA System along the Lowest-Frequency NM
(A–C) Cross-sectional view from within a membrane plane and (D–F) axial view from the IC side. (A and D) the minimized WT KcsA system. (B and E) and (C and F) displacement along seventh NM in the counterclockwise and clockwise directions, respectively. The three helices of each KcsA subunit are shown in backbone representation in the same color. The polypeptide loops are in gray. The pivot points near C termini of the P helices are illustrated for one KcsA subunit (in red) as brown marks with arrows (in black). An enlarged view of a single subunit is shown in Figure S1. The location of A108 at the bundle crossing is marked in black. The water molecules and K^+ ions are shown in the pore. Arrows indicate the directions of rotation and displacement of the KcsA domains upon perturbation. These figures were generated using our Monte Carlo Ion Channel Proteins (MCICP) code.

a concerted, lever-like swinging of the TM2 and TM1 helices (Figure S1, see the Supplemental Data available with this article online, for an expanded view of a single subunit) about pivot points near the C termini of the P helices (Figures 2B and 2C) coupled with concerted rotation of the TM2 bundle around the channel axis (Figures 2E and 2F). This motion fully agrees with NMA of the intrinsic structural flexibility of KcsA (Shen et al., 2002) and NMA of five K^+ channels using coarse-grained models (Shrivastava and Bahar, 2006). For comparison with other studies (Perozo et al., 1999; Liu et al., 2001; Shen et al., 2002; Shrivastava and Bahar, 2006), in what follows, we view all rotations from the IC side. Perturbing along the lowest-frequency NM refers to counterclockwise or clockwise rotation of the TM2 bundle around the channel axis. For counterclockwise (Figure 2E) or clockwise (Figure 2F) rotation of the TM2 bundle, we find that the IC ends of the TM2 helices bend at A108 pivot points toward or away from the pore, respectively. Interestingly, the P helices undergo a swinging motion, but the P loops of the selectivity filter remain nearly rigid. This motion of P helices may be implicated in inactivation of the selectivity filter (Cordero-Morales et al., 2006), an issue that requires a separate study.

Single-Step Atomic Displacements along the Lowest-Frequency NM Eigenvector

We now describe the displacement of the E118p/E120p KcsA atoms in a single-step move in both directions along the lowest-frequency eigenvector to a predefined rmsd in order to generate end-point structures, following protocols used in earlier NMA studies (Shen et al., 2002; Taly et al., 2005; Cheng et al., 2006). Applying an rmsd of 3.5 Å yields a distorted structure with overstretched bonds and steric clashes (the energy increase is >2000 kT, with k, the Boltzmann constant and T, the temperature, 300 K); these are relaxed using a new conjugate gradient method with guaranteed descent (Hager and Zhang, 2005). We find that, when perturbed along the lowest-frequency NM, either counterclockwise or clockwise, the inner hydrophobic vestibule of E118p/E120p KcsA (the region between −20.0 and −5.0 Å) remains closed (Figure 3). There are important structural differences between the narrow vestibule and the pore's central cavity. The wide cavity is water filled, with a K^+ ion resident at its center, while the vestibule, lined by hydrophobic side chains of the TM2 helices, is an inhospitable environment for K^+ ions and water molecules. Comparing the pore radius profile (Shrivastava and Bahar, 2006) or superimposing closed and widened KcsA pores (Liu et al., 2001; Shen et al., 2002) also showed that the narrow inner vestibule only expands marginally. When perturbed counterclockwise, in agreement with earlier theory (Shen et al., 2002), we find that the pore is enlarged in the IC mouth, but remains closed in the inner vestibule (Figure 3, open squares). In a computational study of five K^+ channel structures, with coarse-grained NMA models (Shrivastava and Bahar, 2006), enlargement of the IC end of the pore was observed for rotation in either direction, but the inner vestibule was only widened (~2 Å radius) for rotation in one direction.

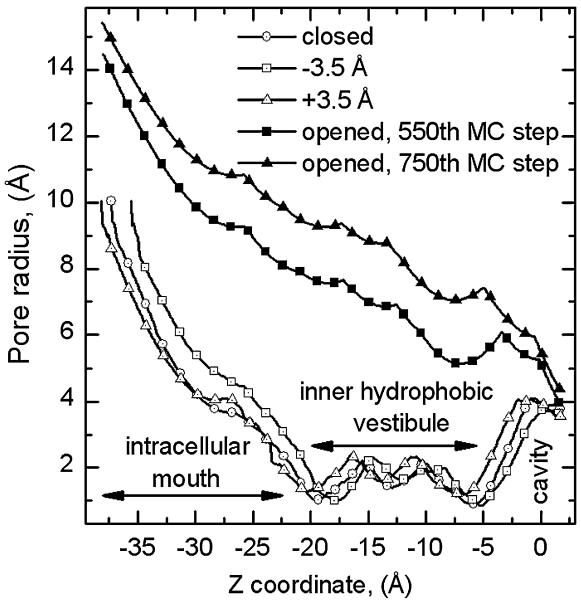

Figure 3. Radius of the IC Pore in the KcsA Channel

The radius is shown as a function of the position along the channel axis for E118p/E120p KcsA. It is computed for the minimized structure (open circles), the perturbed conformations with rmsd of ±3.5 Å (counterclockwise [open squares] and clockwise [open triangles]), and the two opened structures (closed squares and triangles) corresponding to the 550th and 750th MC steps on the transition pathway. The pore radius profiles were generated using our MCICP code.

Perturbing clockwise, we find that the pore is slightly enlarged in the inner vestibule, but the IC mouth is nearly unchanged in size (Figure 3, open triangles). Thus, experiment (Liu et al., 2001), theory (Shen et al., 2002; Shrivastava and Bahar, 2006), and our results (Figure 3) agree that the radius of this opened inner vestibule is ~2 Å. This is nearly as wide as the gA channel, but, being mainly lined with hydrophobic residues, it is an inhospitable environment for both water and K^+ ions. It is thus unclear how K^+ could permeate in single file along the 15 Å length of this enlarged hydrophobic pore (Beckstein and Sansom, 2004).

The Gating Transition in KcsA

What are the conformational changes that lead to opening of the KcsA inner pore? To answer this question, we tracked the lowest-frequency eigenvector by the RTB MC-NMF technique (see Experimental Procedures). In all four protonation variants studied, counterclockwise mode tracking rotated the TM2 bundle so as to tighten the steric closure at the IC mouth. We find that the original tilt, ~25° of TM1 and TM2 (Doyle et al., 1998), increases with respect to the membrane normal. The termini of the TM2 helices bend more noticeably at A108 and point inward toward the pore. Thus, counterclockwise NM tracking does not open the IC pore. It follows a quite different path from that found in our NM perturbation experiments (Figure 3, open squares) and in earlier theoretical studies (Shen et al., 2002; Shrivastava and Bahar, 2006).

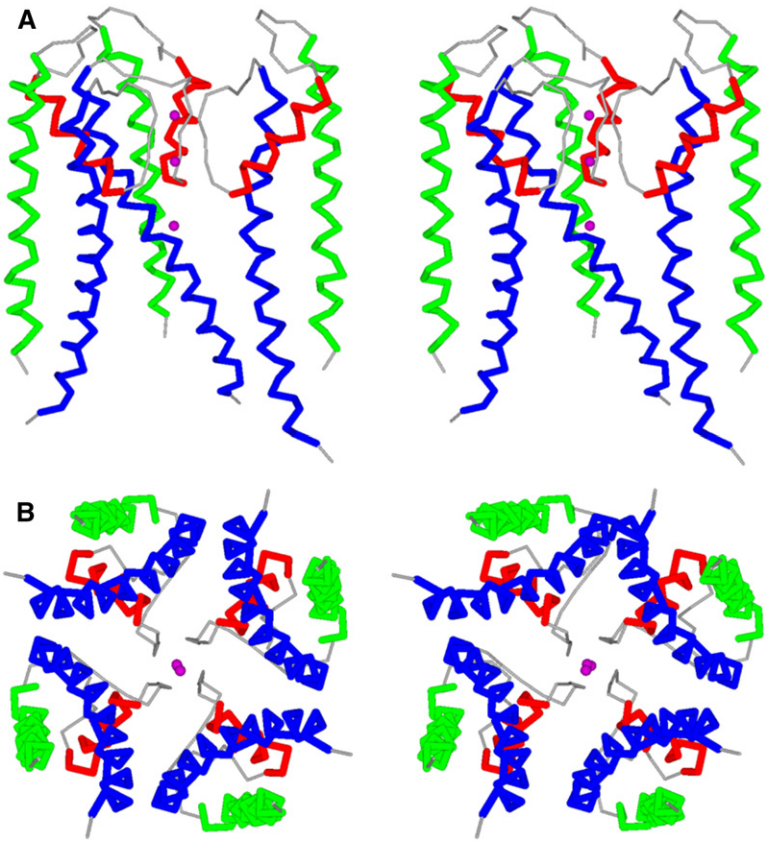

Figure 4. A Stereo Picture of the Backbone of E118p/E120p KcsA in the Open State

View from within the membrane with the extracellular side on top (A) and from the IC side (B). In (A), for clarity, the front subunit is removed. The helices of the KcsA subunits are shown in different colors: TM2 in blue, TM1 in green, and P helix in red. The three K^+ ions in the pore are illustrated as pink spheres. This open-state conformation of KcsA is shown for the 750th MC step.

However, when both E118 and E120 residues are protonated (low interior pH), clockwise mode tracking along the lowest-frequency NM showed a complicated gating transition, with many dynamic features (Movies S1 and S2): (1) concerted rotation and unwinding of the TM2 bundle with an outward bend of TM2 at A108; (2) small twisting-untwisting rotation of the IC end of TM2 about a helical axis; and (3) highly dynamic tilting adjustments and outward lateral motions of TM2 away from the channel axis, leading to the disappearance of the TM2 bundle. The TM2 bundle rotates clockwise ~30°–40° around the channel axis before it becomes disrupted. The tilt of TM1 decreases with respect to the membrane normal as the TM2 bundle is unwound. The TM1 and TM2 helices of each subunit and adjacent subunits dynamically interact with each other during the closed-to-open transition. The cross-section of the inner pore undergoes rapid fluctuations. The large-scale conformational changes are mainly confined to the IC half of the channel, leaving the extracellular half mostly unchanged, supporting the observation that KcsA is a dynamically modular system (Kelly and Gross, 2003). Thus, we find that the gating transition in KcsA is not a simple radial-outward swing (Tikhonov and Zhorov, 2004) of the IC half of the TM2 helices away from the channel axis, bending at the G99 residues. The slotting (clearly visible in the stereo view of Figure 4B) of each TM2 helix (in blue) between two TM1 helices (in green), one from its own subunit and one from an adjacent subunit, and their bend at a gating hinge corresponding to A98–G99, occurs at the end stage of the gating transition (see Figure 4 for the open KcsA conformation). The gating movements are consistent with both spin-labeling (Perozo et al., 1999; Liu et al., 2001) and X-ray (Jiang et al., 2002) experiments: (1) rotation of the TM2 helices is clockwise; (2) the IC end of TM2 is twisted slightly clockwise (~12°) about its helical axis before the TM2 bundle becomes disrupted (Figure S2); and (3) the final TM2 bend is hinged near residues A98–G99. Thus, our results for KcsA, as well as experimental data for *Shaker* and BK channels (Magidovich and Yifrach, 2004), support the idea that TM2 helix deformation in MthK at the conserved glycine (Jiang et al., 2002) might be a common K^+ channel gating mechanism.

The Open-State Conformation of KcsA

The open-state conformation of KcsA exhibits a wide IC pore, with a radius ~5–7 Å in the inner vestibule (Figure 3, closed squares and triangles), located at the constriction near the T107 residues (at −8 Å; see also Figure S3). This is consistent with a radius of about 6 Å at the constriction (at A88) in MthK (Jiang et al., 2002), but is significantly larger than that of about 2 Å at the narrowest point (near residues 107–108) inferred from spin-labeling (Liu et al., 2001) and theoretical (Shen et al., 2002; Shrivastava and Bahar, 2006) studies of KcsA. The size of the wide, open pore increases steadily, starting from the IC entrance of the selectivity filter (the narrowest point) toward the IC side (Figure 3, closed triangles). The IC vestibule is then wide enough for a tetrabutylammonium blocker (TBA)

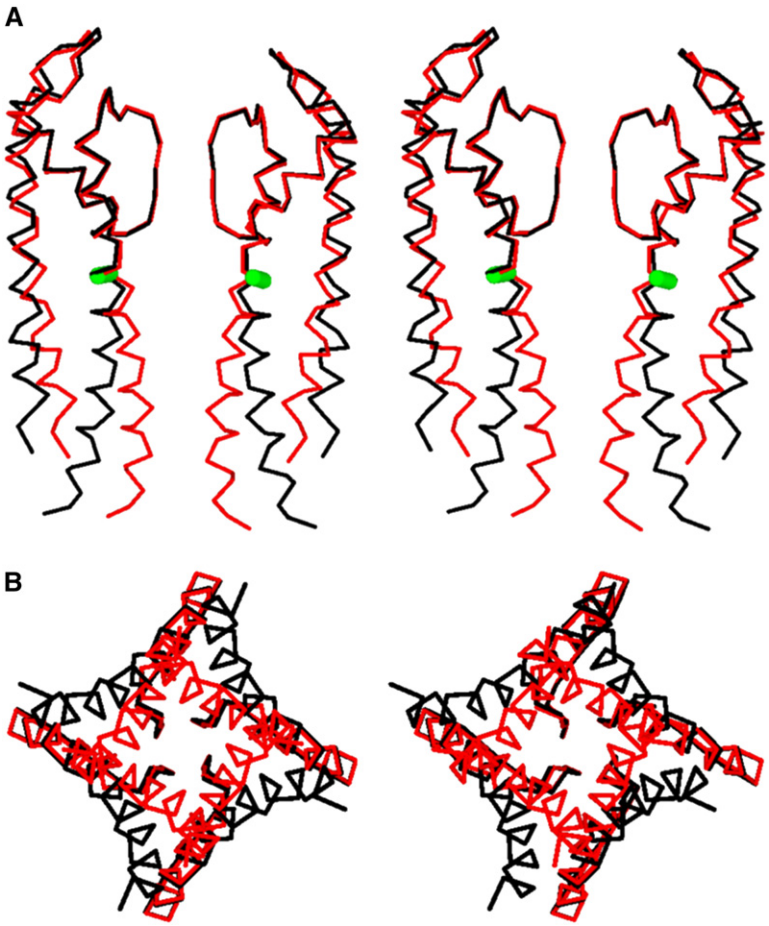

Figure 5. Stereo View of Superimposed Structures of E118p/E120p KcsA

C_α traces are viewed (A) from within the membrane (two subunits) and (B) from the IC side (four subunits). The closed structure is shown in red, and the opened structure is shown in black. The open-state conformation of KcsA is shown for the 650th MC step. The green marks in (A) show the location of a gating hinge, G99. Only the backbone of the selectivity filter and the inner helices is shown in (B). The figures were generated using our MCICP code.

(diameter, 10–12 Å) to reach the central cavity—its binding site—where it was found trapped crystallographically in KcsA-TBA complexes with the IC pore closed (Zhou et al., 2001a; Yohannan et al., 2007). Our results also agree with neutron and X-ray solution scattering experiments (Zimmer et al., 2006), which indicate that the pore's IC mouth diameter widens to ~20–30 Å.

The superimposed, closed and opened KcsA structures are shown in Figure 5. The TM2 helices bend at the A98–G99 hinge (Figure 5A) and rotate clockwise (Figure 5B). This picture agrees with structural data for MthK (Jiang et al., 2002). The selectivity filter P loops are structurally unaffected in the gating process (Figure 5A). In the open conformation, the IC halves of the four TM1 and TM2 helices are loosely coupled and substantially separated from one other. The inner hydrophobic vestibule disappears, and the central cavity becomes an inseparable part of the IC solution. Thus, K^+ ions can traverse half the permeation pathway with a full hydration shell and suffer no energy penalty in reaching the entrance of the selectivity filter.

The Energetics along the Gating Pathway

We find that the energy steadily increases with the number of MC steps along the transition trajectory (Figure 6). As a proper reaction coordinate cannot be identified, we choose the number of MC steps as a continuous variable. After ~550 MC steps, the KcsA channel is trapped in the open conformation illustrated in Figures 4 and 5. The energetics along the gating pathway shown in Figure 6 provide only a qualitative picture, as the effect of surroundings (water and lipids) is not treated in our RTB MC-NMF simulations. This energy profile should be scaled by an effective system dielectric constant (Schutz and Warshel, 2001) in order to include dielectric shielding of electrostatic interactions due to electronic polarization, not incorporated in the force field, and the influence of the reaction fields induced by surrounding electrolyte and membrane. It is known that low-frequency motions in a realistic environment are overdamped and diffusive—not vibrational at all—which makes low-frequency eigenvalues (the energetic cost) of little physical importance. However, low-frequency eigendirections are a unique and inherent property of protein architecture (Lu and Ma, 2005), and there is overwhelming evidence that they are not affected by the presence of solvent (Ma and Karplus, 1997; Ma, 2005) (see also Miloshevsky and Jordan, 2006 and references therein concerning this issue).

The Effect of Protonation of E118 and E120 on the Channel Opening

It is known that KcsA is activated by protons from the IC side of the channel (Heginbotham et al., 1999). It has

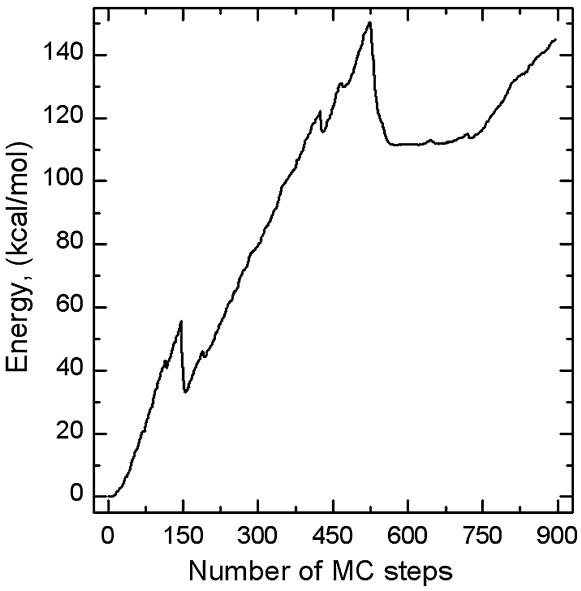

Figure 6. The Energy Profile as a Function of the Number of MC Steps along the Gating Pathway

There is an energy barrier (~150 kcal/mol) for opening the IC pore. The energy well at the ~150th MC step could correspond to a fluctuation or an intermediate, partially stable conformation. The energy profile shows a nearly flat well between the 550th and 750th MC steps. The energy difference from the bottom of the well to the top of the barrier is ~40 kcal/mol, much smaller than that (~110 kcal/mol) from the initial closed state to the final open state.

been suggested that the charged residues (R117, E118, E120, R121, R122, and H124, which is positively charged at acidic pH) of the TM2 helix located near its C terminus constitute the putative pH sensor (Cortes et al., 2001) responsible for triggering channel openings at low pH. The probability that the channel is open increases as pH decreases from pH 7 to pH 4, but it remains quite low (<0.4 under all conditions) (Heginbotham et al., 1999; LeMasurier et al., 2001). Recent experiments (Blunck et al., 2006) suggest that this low open probability reflects the presence of a second gate, located in the selectivity filter; the channel is in a state with an open bundle crossing, but a closed (inactivated) selectivity filter. The charged residues near the C termini of TM2 form a complex inter- and intrasubunit charge network (Figure 7). The RTB MC-NMF simulations reveal that, when both E118 and E120 are in the protonated form (low pH), clockwise NM tracking leads to untwisting of the TM2 helical bundle and a wide open IC pore (Figures 3 and 4). However, we found that, for neutral pH, where the carboxylate groups in both E118 and E120 glutamates are deprotonated, the TM2 bundle undergoes clockwise rotation around the channel axis with backward-forward fluctuations, but no outward-directed movement of its helices away from the pore was observed. In this case, the IC pore remains closed. If either E118 or E120 is protonated, the inner pore radius increases, especially for the E120p variant, but the opening illustrated in Figure 3 is not observed. Protonating E120 and breaking the intersubunit bridges has a larger effect (an inner pore constriction radius of ~3.31 Å) than protonating E118 (an inner pore constriction radius of ~2.15 Å) (Figure 8). Thus, a pH change (protonation of E118 and E120) affects the inter- and intrasubunit electrostatic interactions within the IC domain, initiating a fundamental local architectural change that disrupts at least 8–12 hydrogen bonds. The large net positive charge, due to the arginines located at the ends of the TM2 helices, further promotes destabilization. Their repulsion greatly encourages unwinding the TM2 bundle on the gating pathway, leading to an open state with a very wide IC vestibule.

DISCUSSION

Our MC-NMF analyses of gating pathways in gA (Miloshevsky and Jordan, 2006) and KcsA show that a one-step displacement along the lowest-frequency NM with a predefined rmsd (Shen et al., 2002; Taly et al., 2005; Cheng et al., 2006) is not sufficient to elucidate the gating mechanism. This approach is only valid for identifying the most probable direction for initiating gating. In the gA channel, we found that the lowest-frequency NM corresponds to relative opposed rotation of gA monomers around the channel axis (Miloshevsky and Jordan, 2006). However, this relative rotation did not lead immediately to closing the gA pore or dimer dissociation. Only tracking this lowest-frequency NM with the MC-NMF technique revealed that relative opposed rotation is coupled with subsequent lateral displacement of gA monomers on the gating pathway, which leads to pore closure and dimer dissociation (Miloshevsky and Jordan, 2004, 2006). Displacing the closed KcsA structure along the lowest-frequency NM indicates that channel opening is initiated by rotation of the TM2 bundle around the channel axis. However, we (as well as others [Liu et al., 2001; Shen et al., 2002; Shrivastava and Bahar, 2006]) find that neither counterclockwise nor clockwise perturbation with an rmsd of 3.5 Å fully opens KcsA's inner hydrophobic vestibule. Counterclockwise or clockwise tracking via RTB MC-NMF did not generate a fully open pore in WT, E118p, and E120p KcsA, stressing the important structural consequences of electrostatic effects ignored in elastic network NM models (Shrivastava and Bahar, 2006). The nature and detailed dynamics of the gating transition in KcsA was only revealed by clockwise tracking along the lowest-frequency NM for the low-pH variant where both E118 and E120 are protonated.

In summary, using a novel NM tracking approach, we show that the gating transition in KcsA represents a very large conformational change. The end-point structures are well characterized by rotation-and-tilt and hinge-bending models. Our results argue that neither of the two gating models is incorrect, but that they complement each other, describing the initial and final states on the gating pathway. During the opening, the narrow hydrophobic vestibule is transformed into a very wide domain, fully integrated with the internal solution. This picture has

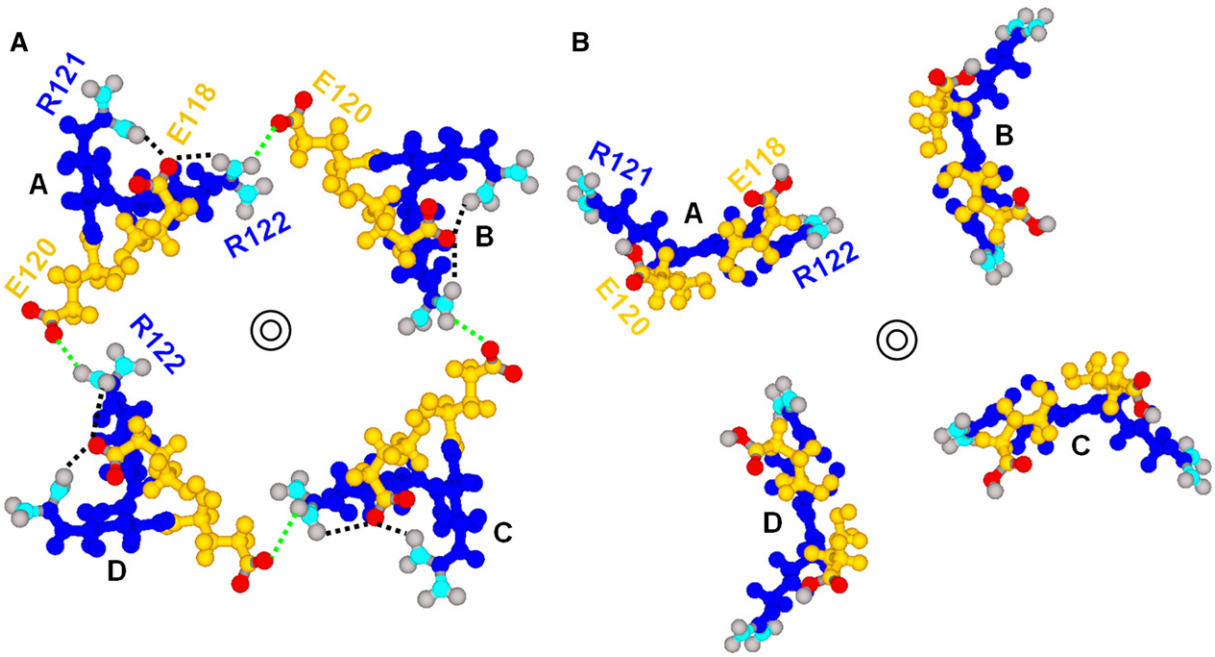

Figure 7. The network of Inter- and Intrasubunit Salt Bridges Formed by Charged Residues in Close Proximity to the C Termini of the TM2 Helices

The network is viewed along the channel axis from the extracellular side in (A) WT KcsA and (B) KcsA with both E118 and E120 protonated. The two concentric circles mark the center of each pore. The KcsA subunits are labeled as A, B, C, and D. The residues are labeled. Arginines and glutamates are shown in blue and gold colors, with their guanidino and carboxyl groups in native colors, respectively. (A) The intersubunit salt bridges between R122 and E120 are shown as green broken lines. The average distance between bridged atoms is 3.2 Å. The intrasubunit bridges between E118 and both R121 and R122 residues are shown as black broken lines. The distance between atoms involved in salt bridges varies between 2.4 and 2.7 Å. (B) The inter- and intrasubunit bridges are broken as a result of glutamate protonation. A proton on one glutamate oxygen is illustrated. There is a significant local architectural change as the side chains of E120 and R121 move radially outward, away from the channel axis.

important implications for our understanding of K^+ permeation. In the open-state conformation, only the narrow selectivity filter constitutes the pore of K^+ channels. Our focus in this study was on conformational changes in the IC domain, and we maintained the E71-D80 constraint in the selectivity filter. Nevertheless, we observed that the gating motions of the IC domain propagate to the selectivity filter. The P helices undergo a swinging motion during the opening of the TM2 bundle, which could affect the putative second gate located in the selectivity filter (Cordero-Morales et al., 2006; Blunck et al., 2006). Further study of the conformational state of selectivity filter P loops in the open KcsA channel with mutations of E71 and D80 is expected to provide more details on the interplay between the two gates.

EXPERIMENTAL PROCEDURES

KcsA Models

The high-resolution KcsA structure (Zhou et al., 2001b) with three K^+ ions and 31 water molecules saturating the cavity and pore domains, termed the KcsA system, was used. KcsA systems were described with the all-hydrogen CHARMM22 topology and parameter set (MacKerell et al., 1998). Protein hydrogens were added by using our Monte Carlo Ion Channel Proteins code. The E71 residues were protonated in order to preserve the carboxy-carboxylate interaction between E71 and D80 and yield a minimized structure mimicking the crystal structure. Unresolved R117 side chains were built, and unresolved H124 residues were not included. The number of atoms as well as NMs is varied depending on the variant. For instance, there are N_a = 6,300 atoms in the WT KcsA system resulting in 18,900 all-atom NMs. The new conjugate gradient method with guaranteed descent (Hager and Zhang, 2005) was used to locate geometry with unprecedented low strain energy for these large molecular systems. The absolute largest component of the gradient $<5 \times 10^{-10}$ kcal mol^{-1} $Å^{-1}$ was reached. All degrees of freedom (bond lengths, bond angles, torsion and improper torsion angles) in both KcsA and the waters were variable during minimization. The rmsd for the C_α atoms was ~1.8 Å between X-ray and WT energy-minimized conformations, and somewhat larger (up to ~2.5 Å) for the protonation variants. Efficient eigensystem solvers from the LAPACK package, as previously described (Miloshevsky and Jordan, 2006), were used to calculate eigenvalues and eigenvectors. The lowest-frequency eigenvalue was varied from 2.2 to 2.9 cm^{-1}, depending on the variant. For comparison, a value of 2.5 cm^{-1} was found in the NMA study of KcsA (Shen et al., 2002).

The RTB MC-NMF Method

The MC-NMF method based on the all-atom NMA is described in detail by Miloshevsky and Jordan (2006). The basis of this method is to systematically maximize the energy along the lowest-frequency NM, while simultaneously minimizing the energy in all other NM directions (Nichols et al., 1990). No constraints, restraints, or artificial internal or external mechanical forces are imposed on the structure while tracking along the lowest-frequency NM. The Metropolis criterion (Metropolis et al., 1953) controls allowable MC step lengths. Each MC step involves the collective motions of large parts of the protein and is characterized by the concerted conformational changes. After each

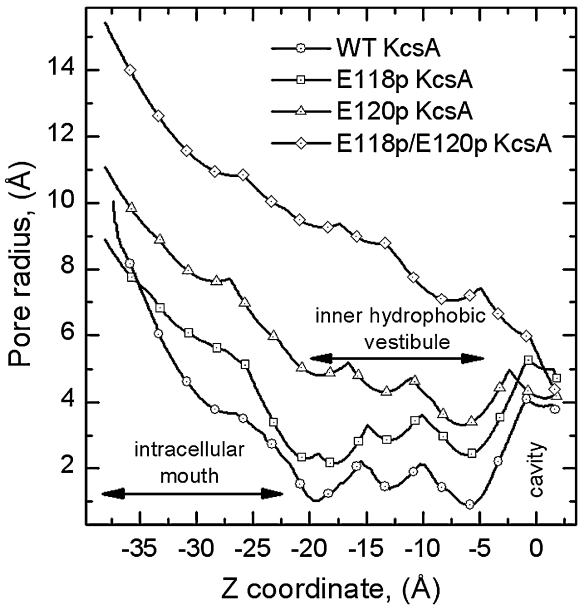

Figure 8. Radius Profiles of the IC Pore for All Four Protonation Variants

WT (circles), E118 KcsA (squares), E120 KcsA (triangles), and E118p/E120p KcsA (diamonds).

accepted step, the all-atom Hessian matrix is recalculated and the eigensystem is solved anew (Nichols et al., 1990)—a very computationally expensive procedure for large proteins. The new lowest-frequency NM that is most similar to the previous one (i.e., has the largest overlap with it) is selected as the degree of freedom to be maximized. Thus, along the gating pathway, the lowest-frequency eigenvector changes with each MC step. After a large number of MC steps, the initial (starting) and current low-frequency NM sets are quite different.

Thus, tracking along the lowest-frequency NM in KcsA requires a multiple recalculation of the Hessian matrix and resolution of the eigensystem (~500–900 steps). We find that direct application of MC-NMF to the KcsA system is not feasible, as the computational cost associated with one-step diagonalization of the all-atom Hessian matrix (size $3N_a \times 3N_a$) with the most efficient solver from LAPACK is ~17 hr on a Dell dual 3.8 GHz workstation with 12 GB of memory. The memory requirements are about 4.4 GB for storing the Hessian matrix and eigenvectors. Therefore, instead of the all-atom NMs, we incorporated RTB NMs (Tama et al., 2000) into the MC-NMF technique. The justification for using RTB NMs is that the low-frequency NMs are very close to one another in both approaches. In the RTB approximation (Tama et al., 2000), an all-atom Hessian is projected onto a space spanned by the rotational and translational degrees of freedom of predefined protein blocks, thus effectively reducing the Hessian matrix (to a size of $6n_b \times 6n_b$, with n_b number of blocks) and the diagonalization time. For each KcsA residue, a peptide backbone was treated as a single block, and the side chain was broken into zero (glycine and proline) to three (arginine and lysine) blocks, depending on residue size. The water molecules were treated as separate blocks, and K^+ ions were associated with nearby blocks. For instance, there are $n_b = 1211$ rigid blocks in the WT KcsA system (7266 RTB NMs), requiring ~1 hr of diagonalization time. The $6n_b$ length RTB NMs are then projected back to all-atom space to give a limited number, $6n_b$, of the full-length ($3N_a$) approximate all-atom NMs. It is important to choose the number of blocks such that the largest eigenvalue is close to ~1300 cm^{-1}, fully covering the vibrations of single amino acids (torsional subspace) (see the NM spectrum in Figure 1). When the true all-atom NMs are substituted by the approximate all-atom NMs derived from the RTB approach, we find that the standard MC-NMF method (Miloshevsky and Jordan, 2006) fails. There are a limited number of approximate NMs resulting in insufficient relaxation of the high-frequency NM subspace. A solution was found by separating the maximization step along the lowest-frequency NM from the minimization step along the other NMs. In our original MC-NMF method (Miloshevsky and Jordan, 2006), these two steps are carried out simultaneously (Nichols et al., 1990). For each accepted maximization step, the minimization step along the other NMs is now repeated many times until the simulational system is totally relaxed. Thus, a single MC move (step) along the lowest-frequency NM includes the maximization step and a number of minimization steps. This modified MC-NMF method is reminiscent of our kinetic approach (Miloshevsky and Jordan, 2005); in both, motion is unidirectionally constrained along a predefined reaction coordinate, and many MC trials are performed to relax the other degrees of freedom after each step along the reaction coordinate. The RTB MC-NMF method, before its application to the KcsA systems, was extensively tested and shown to reproduce the gating transitions in the gA channel (Miloshevsky and Jordan, 2004, 2006).

Supplemental Data

Supplemental Data include three figures and two movies and are available online at http://www.structure.org/cgi/content/full/15/12/1654/DC1/.

ACKNOWLEDGMENTS

We thank C. Miller, R. MacKinnon, and J. Ma for useful communications. This work was supported by National Institutes of Health grant GM-28643.

Received: August 15, 2007
Revised: September 28, 2007
Accepted: September 30, 2007
Published: December 11, 2007

REFERENCES

Achterhold, K., Keppler, C., Ostermann, A., van Bürck, U., Sturhahn, W., Alp, E.E., and Parak, F.G. (2002). Vibrational dynamics of myoglobin determined by the phonon-assisted Mössbauer effect. Phys. Rev. E Stat. Nonlin. Soft Matter Phys. *65*, 051916. Published online May 17, 2002. 10.1103/PhysRevE.65.051916.

Beckstein, O., and Sansom, M.S.P. (2004). The influence of geometry, surface character and flexibility on the permeation of ions and water through biological pores. Phys. Biol. *1*, 42–52.

Blunck, R., Cordero-Morales, J.F., Cuello, L.G., Perozo, E., and Bezanilla, F. (2006). Detection of the opening of the bundle crossing in KcsA with fluorescence lifetime spectroscopy reveals the existence of two gates for ion conduction. J. Gen. Physiol. *128*, 569–581.

Cheng, X., Lu, B., Grant, B., Law, R.J., and McCammon, J.A. (2006). Channel opening motion of α7 nicotinic acetylcholine receptor as suggested by normal mode analysis. J. Mol. Biol. *355*, 310–324.

Cordero-Morales, J.F., Cuello, L.G., Zhao, Y., Jogini, V., Cortes, D.M., Roux, B., and Perozo, E. (2006). Molecular determinants of gating at the potassium-channel selectivity filter. Nat. Struct. Mol. Biol. *13*, 311–318.

Cortes, D.M., Cuello, L.G., and Perozo, E. (2001). Molecular architecture of full-length KcsA: role of cytoplasmic domains in ion permeation and activation gating. J. Gen. Physiol. *117*, 165–180.

Cuello, L.G., Romero, J.G., Cortes, D.M., and Perozo, E. (1998). pH-dependent gating in the *Streptomyces lividans* K^+ channel. Biochemistry *37*, 3229–3236.

Doyle, D.A., Cabral, J.M., Pfuetzner, R.A., Kuo, A., Gulbis, J.M., Cohen, S.L., Chait, B.T., and MacKinnon, R. (1998). The structure of

the potassium channel: molecular basis of K^+ conduction and selectivity. Science *280*, 69–77.

Hager, W.W., and Zhang, H. (2005). A new conjugate gradient method with guaranteed descent and an efficient line search. SIAM J. Optim. *16*, 170–192.

Heginbotham, L., LeMasurier, M., Kolmakova-Partensky, L., and Miller, C. (1999). Single *Streptomyces lividans* K^+ channels: functional asymmetries and sidedness of proton activation. J. Gen. Physiol. *114*, 551–560.

Jiang, Y., Lee, A., Cadene, M., Chait, B.T., and MacKinnon, R. (2002). The open pore conformation of potassium channels. Nature *417*, 523–526.

Kelly, B.L., and Gross, A. (2003). Potassium channel gating observed with site-directed mass tagging. Nat. Struct. Biol. *10*, 280–284.

LeMasurier, M., Heginbotham, L., and Miller, C. (2001). KcsA: it's a potassium channel. J. Gen. Physiol. *118*, 303–314.

Levitt, M., Sander, C., and Stern, P.S. (1985). Protein normal-mode dynamics: trypsin inhibitor, crambin, ribonuclease and lysozyme. J. Mol. Biol. *181*, 423–447.

Liu, Y.S., Sompornpisut, P., and Perozo, E. (2001). Structure of the KcsA channel intracellular gate in the open state. Nat. Struct. Biol. *8*, 883–887.

Lu, M., and Ma, J. (2005). The role of shape in determining molecular motions. Biophys. J. *89*, 2395–2401.

Ma, J. (2005). Usefulness and limitations of normal mode analysis in modeling dynamics of biomolecular complexes. Structure *13*, 373–380.

Ma, J., and Karplus, M. (1997). Ligand-induced conformational changes in *ras* p21: a normal mode and energy minimization analysis. J. Mol. Biol. *274*, 114–131.

MacKerell, A.D., Jr., Bashford, D., Bellott, M., Dunbrack, R.L., Jr., Evanseck, J.D., Field, M.J., Fischer, S., Gao, J., Guo, H., Ha, S., et al. (1998). All-atom empiricalpotential for molecular modeling and dynamics studies of proteins. J. Phys. Chem. B *102*, 3586–3616.

Magidovich, E., and Yifrach, O. (2004). Conserved gating hinge in ligand- and voltage-dependent K^+ channels. Biochemistry *43*, 13242–13247.

Metropolis, N., Rosenbluth, A.W., Rosenbluth, M.N., Teller, A.H., and Teller, E. (1953). Equation of state calculations by fast computing machines. J. Chem. Phys. *21*, 1087–1091.

Miloshevsky, G.V., and Jordan, P.C. (2004). Gating gramicidin channels in lipid bilayers: reaction coordinates and the mechanism of dissociation. Biophys. J. *86*, 92–104.

Miloshevsky, G.V., and Jordan, P.C. (2005). Permeation and gating in proteins: kinetic Monte Carlo reaction path following. J. Chem. Phys. *122*, 214901–214907.

Miloshevsky, G.V., and Jordan, P.C. (2006). The open state gating mechanism of gramicidin A requires relative opposed monomer rotation and simultaneous lateral displacement. Structure *14*, 1241–1249.

Nichols, J., Taylor, H., Schmidt, P., and Simons, J. (1990). Walking on potential energy surfaces. J. Chem. Phys. *92*, 340–346.

Perozo, E., Cortes, D.M., and Cuello, L.G. (1999). Structural rearrangements underlying K^+-channel activation gating. Science *285*, 73–78.

Perozo, E. (2002). New structural perspectives on K^+ channel gating. Structure *10*, 1027–1029.

Schutz, C.N., and Warshel, A. (2001). What are the dielectric "constants" of proteins and how to validate electrostatic models? Proteins Struct. Funct. Genet. *44*, 400–417.

Shen, Y., Kong, Y., and Ma, J. (2002). Intrinsic flexibility and gating mechanism of the potassium channel KcsA. Proc. Natl. Acad. Sci. USA *99*, 1949–1953.

Shrivastava, I.H., and Bahar, I. (2006). Common mechanism of pore opening shared by five different potassium channels. Biophys. J. *90*, 3929–3940.

Taly, A., Delarue, M., Grutter, T., Nilges, M., Le Novere, N., Corringer, P.J., and Changeux, J.P. (2005). Normal mode analysis suggests a quaternary twist model for the nicotinic receptor gating mechanism. Biophys. J. *88*, 3954–3965.

Tama, F., Gadea, F.X., Marques, O., and Sanejouand, Y.H. (2000). Building-block approach for determining low-frequency normal modes of macromolecules. Proteins Struct. Funct. Genet. *41*, 1–7.

Tikhonov, D.B., and Zhorov, B.S. (2004). In silico activation of KcsA K^+ channel by lateral forces applied to the C-termini of inner helices. Biophys. J. *87*, 1526–1536.

Valadie, H., Lacapcre, J., Sanejouand, Y., and Etchebest, C. (2003). Dynamical properties of the MscL of *Escherichia coli*: a normal mode analysis. J. Mol. Biol. *332*, 657–674.

Yohannan, S., Hu, Y., and Zhou, Y. (2007). Crystallographic study of the tetrabutylammonium block to the KcsA K^+ channel. J. Mol. Biol. *366*, 806–814.

Zhou, M., Morals-Cabral, J.H., Mann, S., and MacKinnon, R. (2001a). Potassium channel receptor site for the inactivation gate and quaternary amine inhibitors. Nature *411*, 657–661.

Zhou, Y., Morais-Cabral, J.H., Kaufman, A., and MacKinnon, R. (2001b). Chemistry of ion coordination and hydration revealed by a K^+ channel-Fab complex at 2.0 Å resolution. Nature *414*, 43–48.

Zimmer, J., Doyle, D.A., and Grossmann, J.G. (2006). Structural characterization and pH-induced conformational transition of full-length KcsA. Biophys. J. *90*, 1752–1766.

Structure *15*

Supplemental Data

Open-State Conformation of the KcsA K^+ Channel: Monte Carlo Normal Mode Following Simulations

Gennady V. Miloshevsky and Peter C. Jordan

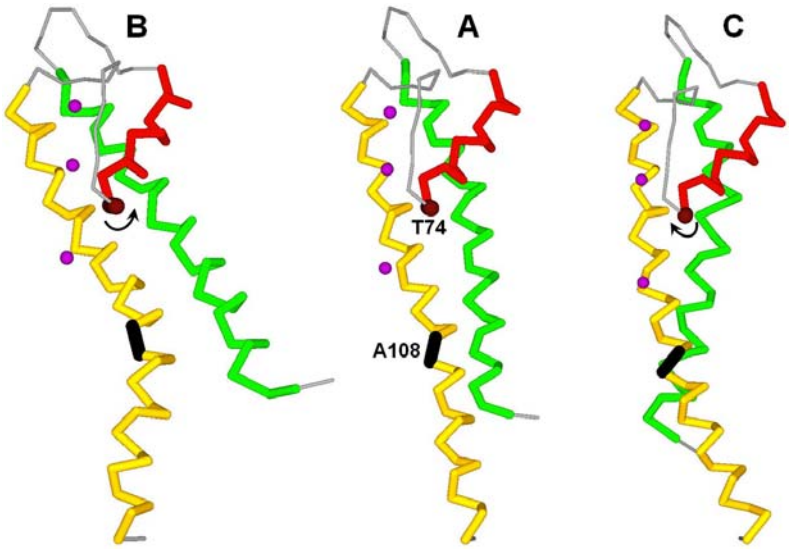

Figure S1. Perturbation of a Single Subunit along the Lowest-Frequency (7^{th}) NM

(A-C) Cross-sectional view from within a membrane plane as seen by an observer on the pore axis. (A) the minimized KcsA subunit. (B) and (C) displacement along 7^{th} NM in the anticlockwise and clockwise directions, respectively. The helices are shown in different colors: TM2 in yellow, TM1 in green and P-helix in red. The polypeptide loops are in grey. The pivot points near C-termini of the P-helices (near T74) are illustrated as brown marks. Black arrows indicate the directions of concerted rotation of TM2 and TM1 around this point upon perturbation. The P-helix undergoes a small swinging motion. The location of A108 at the bundle crossing is marked in black. Upon perturbation TM2 develops a kink at this point. K^+ ions are shown in pink.

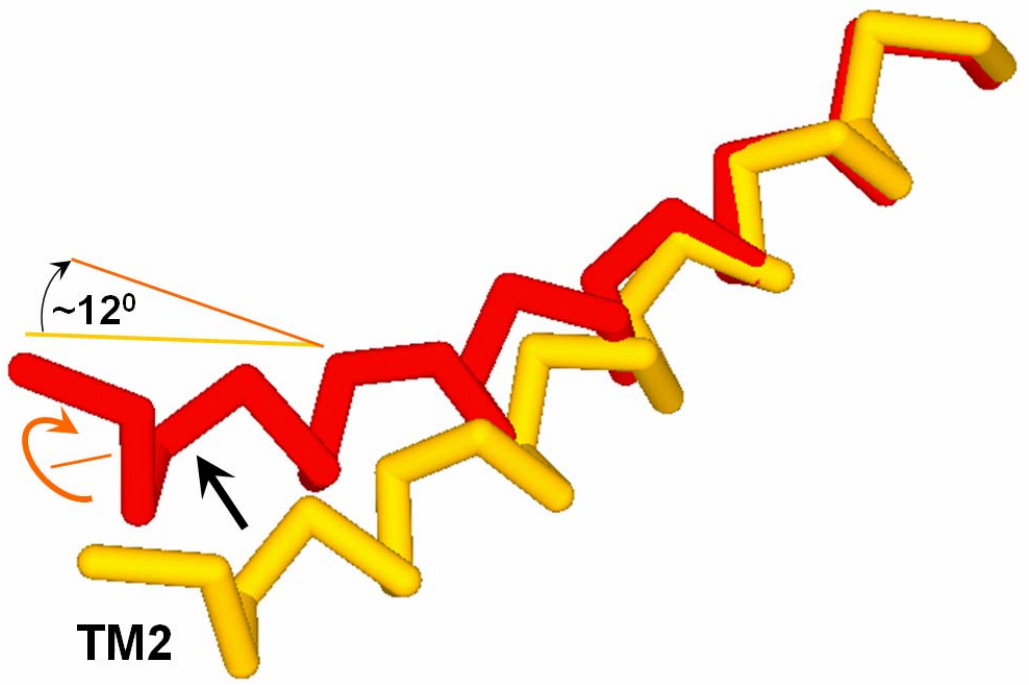

Figure S2. The Initial Conformational Rearrangements in TM2 on the Transition Pathway from the Closed to the Open State

TM2 (gold) tilts away from the channel axis (black arrow) and initiates a clockwise twisting rotation of its C-terminus about the helical axis (red arrow), when viewed from the intracellular side. The twist angle varies along the length of TM2. It is zero near the selectivity filter (on the right) and fluctuates on the gating pathway around ~0^0-12^0 at the C-terminus (on the left). The conformation of TM2 (red) is shown for 230^{th} MC step when the TM2 bundle disappears.

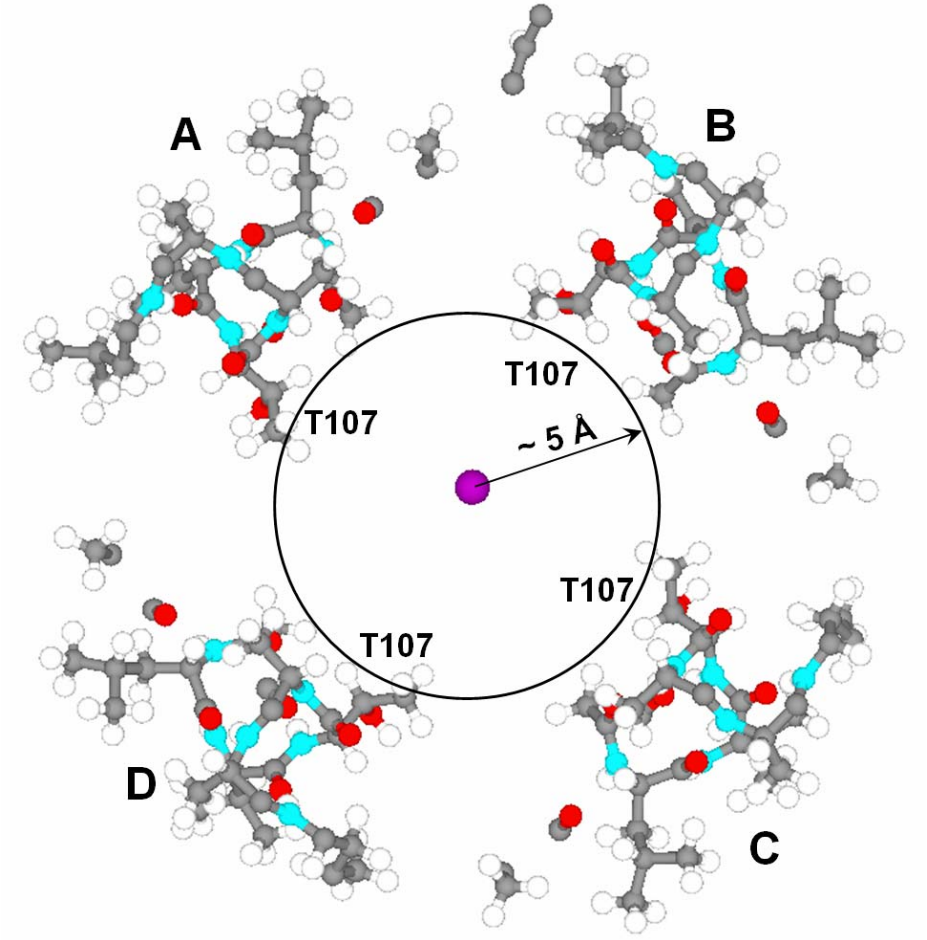

Figure S3. The Size of the Pore in the Inner Hydrophobic Vestibule of E118p/E120p KcsA at the Constriction near the T107 Residues

The nearby atoms of the four KcsA subunits (labeled as **A**, **B**, **C** and **D**) are shown in native colors. The T107 residues are labeled. The K^+ ion located at the narrowest point is a pink sphere. This conformation, constriction radius ~5 Å, is illustrated for the 550^{th} MC step.